EVOLUTION OF THE SUN'S NEAR-SURFACE ASPHERICITIES OVER THE ACTIVITY CYCLE

P.R. Goode[1], L.V. Didkovsky[1], K.G. Libbrecht[2], and M.F. Woodard[1]

[1]*Big Bear Solar Observatory, New Jersey Institute of Technology, Big Bear City, CA 92314, USA*
[2]*Physics Department, California Institute of Technology, Pasadena, CA 91125, USA*

ABSTRACT

Solar oscillations provide the most accurate measures of cycle dependent changes in the sun, and the Solar and Heliospheric Observatory/Michelson Doppler Imager (MDI) data are the most precise of all. They give us the opportunity to address the real challenge – connecting the MDI seismic measures to observed characteristics of the dynamic sun.

From inversions of the evolving MDI data, one expects to determine the nature of the evolution, through the solar cycle, of the layers just beneath the sun's surface. Such inversions require one to guess the form of the causal perturbation – usually beginning with asking whether it is thermal or magnetic. Matters here are complicated because the inversion kernels for these two are quite similar, which means that we don't have much chance of disentangling them by inversion. However, since the perturbation lies very close to the solar surface, one can use synoptic data as an outer boundary condition to fix the choice. It turns out that magnetic and thermal synoptic signals are also quite similar. Thus, the most precise measure of the surface is required.

We argue that the most precise synoptic data come from the Big Bear Solar Observatory (BBSO) Solar Disk Photometer (SDP). A preliminary analysis of these data implies a magnetic origin of the cycle-dependent sub-surface perturbation. However, we still need to do a more careful removal of the facular signal to determine the true thermal signal.

INTRODUCTION

As a spin-off from the Princeton oblateness observations (Kuhn, Libbrecht and Dicke 1988, and references therein), large scale, small amplitude asphericities were discovered by Kuhn (1988) in solar limb brightness observations. The asphericities took the form of latitudinal intensity or "temperature" (as denoted by Kuhn) bands. Kuhn also noted that the asphericities were dramatically changing with the solar cycle and roughly associated with the active latitudes. Further, he linked the evolving systematics of these aspericities with those in the asphericities in the fine structure in the spectrum of solar oscillations.

This picture was strongly confirmed by Libbrecht and Woodard (1990) and Woodard and Libbrecht (1991) who compared the asymmetric parts of their 1986 and 1988 splitting data from Big Bear Solar Observatory (BBSO). They noted significant changes in centroid frequencies, $\bar{\nu}_{\ell,n}$ (which reflect surface averaged changes in the sun), and the coefficients describing the asymmetric part of the fine structure, $a_{2k,\ell}$ (the so-called even-a coefficients). They showed that both quantities scale inversely as the mode inertia (mass). This finding implied that the site of the perturbation giving rise to changes is located in the outer part of the sun. Furthermore, they demonstrated that the angular dependence of the perturbation causing the asymmetry in the splittings is similar to the latitudinal dependence of the active latitudes *and* intensity or "temperature" bands.

The sources of the changes are generally considered to be some combination of variations in temperature, magnetic field and changes in the random velocity field. However, it has been established beyond a reasonable

doubt that there is a close association among the evolution of the "temperature" bands, active latitudes and the aforementioned changes in the p-mode spectrum. *But precisely what effect of activity are the p-modes reflecting?*

The direct source of the cycle dependent changes has been a matter of controversy. However, the only well-established changes are dominated by effects arising in the outermost layers of the sun. The oscillations strongly sample this region and, as detected by MDI, are ideal probes.

Bachmann and Brown(1993) demonstrated a strong correlation among the centroid shifts and various characteristics of activity, including the Mg II 280 nm core-to-wing ratio, the 10.7 cm radio flux, the He I 10830 Å index, the Kitt Peak magnetic index, the EUV flux, and the Magnetic Plage Index Strength. A similar analysis for the new cycle based on GONG data has been presented by Bhatnagar, Jain and Tripathy (1999) in which they find a strong correlation to most of the characteristic indices of activity. They used essentially the same indices as Bachmann and Brown. A similar result was obtained from GONG data by Howe, Komm and Hill (1999), but their results extend over a longer time interval.

Dziembowski and Goode (1991) studied the asymmetry in detail, and they were able to localize the site of the perturbation to be *very near the surface.* They considered the Lorentz force arising from the fibril fields to be the cause of the perturbation. Also, Goldreich, et al. (1991) reached a similar conclusion concerning localization of the source of the frequency perturbation varying with the solar cycle. For their argument, they analyzed the data on centroid shifts from the BBSO measurements. Overall, treating the interaction of oscillations with the fibril fields is a difficult problem and our understanding of it is far from complete (Rosenthal 1995, Rosenthal and Gough 1989 and Zweibel and Däppen 1989).

Goldreich, et al. (1991) specifically proposed that changes in the superficial, random magnetic field are the primary cause of the centroid frequency shifts. This idea has been criticized by Kuhn (1998) who points out that Goldreich, et al. require a mean, quadratic, near-surface magnetic perturbation, $< B^2 >$ of around $(250G)^2$, while the observations of Lin (1995) and Lin and Rimmele (1999) show a mean, surface field which is significantly weaker ($< B^2 > \sim (70G)^2$). Instead, Kuhn sees a critical role for the variations of the Reynold's stresses or turbulent pressure through the solar cycle .

Kuhn proposes that changes in the aspherical component of the stresses are responsible for the varying even-a coefficients. In his picture, the effect of the frequency change arises near the surface, but the asphericity has its source at the base of the convective zone. This is plausible. However, there is strong evidence that both the centroid and even-a frequency changes closely reflect changes in the magnetic field. In particular, Dziembowski et al. (2000), hereafter DGKS, demonstrated that the evolving asphericities in the even-$a's$ are closely mimicked by the corresponding ones found in the BBSO Ca II K data. One possible way of evading the apparent contradiction Kuhn raises would be to contemplate a significant inward increase in the field intensity. *We emphasize that in discussing the field, one has to be careful to distinguish among the direct mechanical effect of the Lorentz force, and the thermal effect arising from the annihilation of the field (referred to as the β-effect) and the force's indirect effect on the thermal structure through the perturbation of the convective transport (referred to as the α-effect).* Only the latter effect may be significant and play a role in the irradiance changes (e.g., Spruit 1998).

Clearly, we are lacking a basic understanding as to how the frequency changes arise. We need more observational information. The most crucial time period for which we need data is during the rise and through the maximum of the cycle. Fortunately, we will have MDI data covering that period for the current cycle, including 18 months of the most recent MDI data ready for examination.

CYCLE VARIATION SEEN FROM MDI DATA

The MDI oscillation data consist of a series of 72-daylong sets. The first eleven are consecutive and cover the period beginning 1996 May 1 and ending 1998 May 31. The remainder begin after SOHO operation was recovered, and begin with a set covering 1999 Feb. 3 - 1999 April 15. To date, each contains a centroid frequency, $\bar{\nu}_{\ell,n}$, and 36 splitting coefficients, a_k. Each set contains between 1620 and 1680 p-mode multiplets (or ℓ-values from 1 up to 200) and between 120 and 143 f-mode multiplets (of ℓ-values from 123 up to 300).

For each p-mode multiplet, the individual mode frequencies, $\nu_{\ell,n,m}$, are represented by

$$\nu_{\ell,n,m} - \bar{\nu}_{\ell,n} = \sum_{k=1} a_k \mathcal{P}_k^\ell(m), \tag{1}$$

where $\mathcal{P}$ are orthogonal polynomials (see Ritzwoller and Lavely 1991 and Schou et al. 1994). This representation ensures that the $\bar{\nu}_{\ell,n}$ are a probe of the spherical structure while the a_{2k} – the even-a coefficients – are a sensitive probe of the symmetrical (about the equator) part of distortion described by the corresponding $P_{2k}(\cos\theta)$ Legendre polynomials. We have

$$C_{k\ell}\mathcal{P}_{2k}^\ell(m) = \int_0^{2\pi}\int_{-1}^{1} |Y_\ell^m|^2 P_{2k} d(\cos\theta) d\phi, \tag{2}$$

where the geometric coefficients, C, are

$$C_{k\ell} = (-1)^k \frac{(2k-1)!!}{k!} \frac{(2\ell+1)!!}{(2\ell+2k+1)!!} \frac{(\ell-1)!}{(\ell-k)!}. \tag{3}$$

We only consider p-modes. The p and f modes have different properties in the outer layers.

DGKS determined the γ_k from the even-order splitting coefficients in each of the datasets using the following formula that was derived under quite general considerations (Dziembowski and Goode, 1991)

$$a_{2k(\ell n)} = a_{2k(\ell n)\mathrm{rot}} + C_{k\ell}\frac{\gamma_k}{I_{\ell n}}, \tag{4}$$

where $a_{2k(\ell n)\mathrm{rot}}$ represents the effect of centrifugal distortion, which DGKS calculated from the SOHO/MDI data following the treatment of Dziembowski and Goode (1992); $I_{\ell n}$ is a measure of the modal inertia (also called the mode mass), and γ_k is the asphericity coefficient corresponding to a P_{2k} distortion – the quantity we are trying to determine. The γ_k are a weak function of frequency. To study the temporal variation of the asymmetry, DGKS therefore eliminated the constant distortion of rotation from the γ coefficients in equation (4). The modal inertia was evaluated assuming that all modes have the same radial displacement at the base of solar photosphere. The inertia decreases with increasing ℓ or n. Equation (4) can also be used to represent changes in centroid frequencies. However, in that case one can determine only a relative γ_0. For this, DGKS chose the first (earliest) of the MDI sets as the reference.

The $I_{\ell n}^{-1}$ factor accounts for most of the, fairly strong, ℓ and frequency dependence in the splitting coefficients. This result is due to Libbrecht and Woodard (1990). They used it as evidence that the asphericity responsible for the even-a coefficients is localized well above the lower turning point of modes in the sample – that is, close to the surface. Dziembowski and Goode (1991) were able to determine a slight, but significant ν-dependence of the γ_1 and γ_2 coefficients from the same data.

In Figure 1, we show the first twelve γ coefficients derived from the SOHO/MDI instrument. This figure is Figure 1 in DGKS. We see clear trends in γ_0, γ_1, γ_2, γ_3, γ_4 and γ_5. Beyond P_{10}, there is not always a clear trend, although P_{14} and P_{16} are fairly suggestive. We note that the errors are rapidly increasing with order, k. In detail, the error bars through P_{12} are inside the symbol. The errors increase with order, but even for P_{24} the error bars span only 4×10^{-2} μHz. Even there, the values are marginally significant, although there is not a clear trend for the P_{24}. Most analyses have focussed on the first few coefficients in the expansion.

In Figure 2, we show the temporal evolution of the $\gamma's$ over thirteen years. This is Figure 6 of DGKS. The mean values of the γ coefficients were determined from equation (4) using data from various sources including BBSO, LOWL and SOHO/MDI. The BBSO data are from Woodard and Libbrecht (1991), and LOWL data are from Tomczyk (1996). We compare the $\gamma's$ with the monthly averages of smoothed sunspot numbers. Roughly, the BBSO data of the summer of 1989 give the largest magnitudes of the $\gamma's$, and this corresponds to the first half of the previous sunspot maximum. Unfortunately, we are missing splitting data from the rising phase (1987 or so), as well as from the declining phase of the solar cycle. Furthermore, the data are seasonal. The errors in the BBSO and LOWL $\gamma's$ are about twice as large as those in SOHO/MDI, but they are still relatively small and would not be visible in Figure 2.

For solar cycle 23, the rapid rise through early 1999, especially of the P_6 coincides with the rise of the sunspot number. Based on a comparison with the previous maximum, it can be noted that the maximum

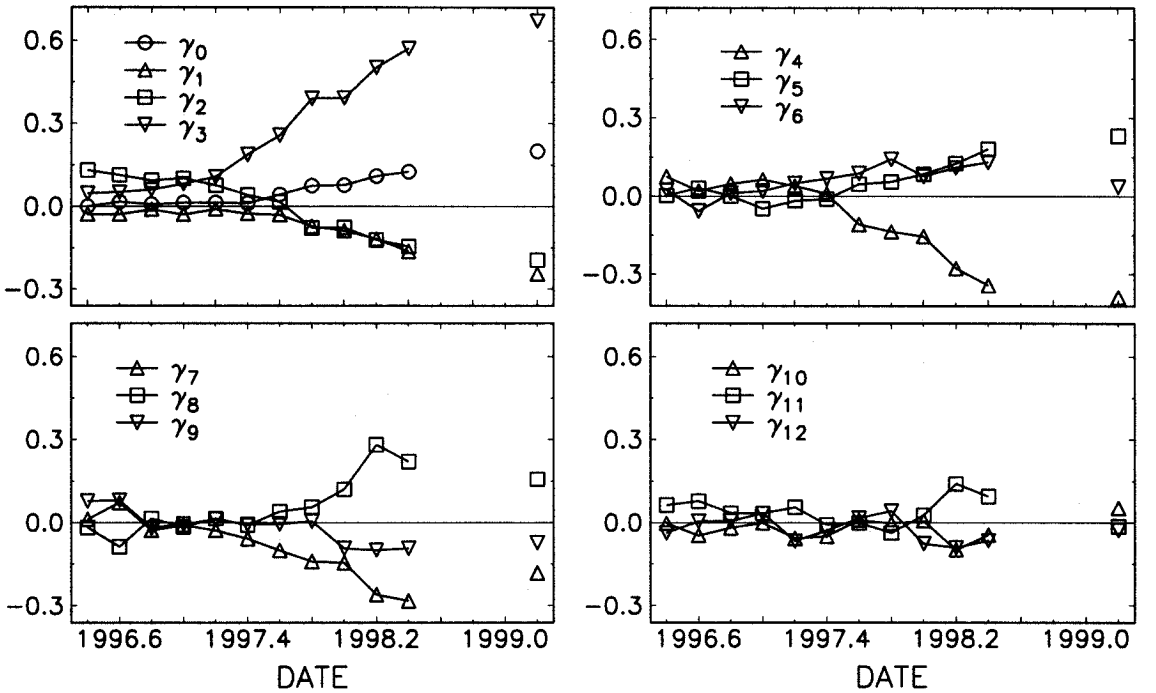

Fig. 1. Mean asphericity coefficients, γ, (in μHz) from the first twelve SOHO/MDI 72-day sets (Schou 1999). The first eleven were obtained consecutively during the first two years of SOHO observations (1996 May 1 - 1998 May 31). The twelfth covers 1999 Feb. 3 - 1999 April 15. For γ_0 through γ_6, the error bars are within the symbols. The errors increase with order, but even for γ_{12} the error bars span only 4×10^{-2} μHz.

value of γ_3 (at 1999.2) corresponds to a much higher activity level than reflected in the sunspot number. The difference can only be partially explained by the difference in mode sets used to infer the γ in the BBSO and MDI sets. There is some sensitivity of the inferred γ's to the maximum ℓ in the set. The maximum ℓ in the MDI sets is between 197 and 200, while for the BBSO sets, it is 140. DGKS found that by truncating the MDI data, they determined absolute values that are a few percent lower (typically 1-3 %).

Thus, from Figure 2, the MDI γ's from early 1999 look closest to their BBSO counterparts from the last activity maximum at the peak of solar activity. However, the sunspot numbers in early 1999 are a mere fraction of those at the maximum of cycle 22. Since many believe the γ's are directly magnetic in origin, the similarities between the sunspot numbers compared to the discrepancies of the γ's are perplexing. This, in itself, motivates comparison among the evolving, continuous MDI oscillation spectrum and various, evolving measures of surface magnetic and intensity or "thermal" effects. We believe that synoptic measures are essential to guiding inversions to determine the nature of the causal, near-surface perturbation.

PROBLEMS WITH INVERTING FOR INTERIOR SIGNATURE OF CYCLE VARIABILITY

The main advantage of a helioseismic probing of solar variability over the cycle is the prospect of detecting changes beneath the photosphere. There is strong evidence that most of the signal one sees in the $\gamma's$ arises close to the surface. One needs to determine by inversion exactly how close, and whether or not one can see a signal from deeper layers. Such inversions require one to *guess the form* of the perturbation and then *invert for its properties.*

DGKS developed formulae connecting the magnetic field and the resulting perturbation of the thermodynamical quantities, and their combined effect on the oscillation frequencies. Furthermore, they considered the θ-dependence of the mean magnetic field which enabled them to develop corresponding connection formulae for the even a-coefficients.

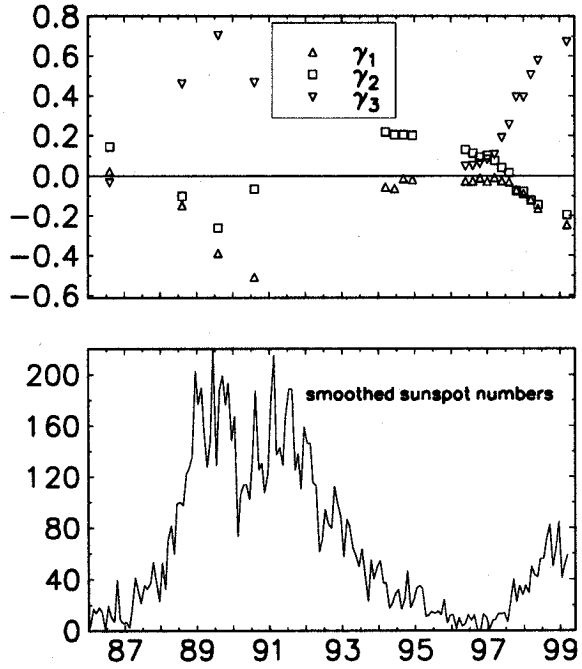

Fig. 2. Lower panel shows the monthly averages of the sunspot number covering the period from 1986 through early 1999. Upper panel shows the mean $\gamma's$ (μHz), from DGKS, covering from 1986 through early 1999. The first cluster of points is from BBSO data (1986-1990). The second is LOWL (1994) and the third is the twelve MDI data sets.

DGKS assumed the *form* of the perturbation is described by an isotropic, random field. Specifically, they set

$$\overline{B_i B_j} = \frac{B^2(r,\theta)}{3}\delta_{ij}, \tag{5}$$

where the quantities in the formula have their usual meanings. Then, we represent B^2 in the form

$$B^2(r,\theta) = 24\pi \sum h_k(r) P_{2k}(\cos\theta). \tag{6}$$

There are important physical distinctions resulting from the differences between the spherical and non-spherical parts of the perturbation. For the spherical part, the connection between h_k and the corresponding thermodynamical parameters requires that one consider the star's thermal balance. For the non-spherical part, mechanical equilibrium conditions alone suffice. For the inversion formalism, this means that for the spherically symmetric perturbation one has to consider two unknown structural functions, u_0 (where $u = \frac{P}{\rho}$) and h_0. DGKS identified these two unknown functions with the differences between the current and the solar minimum values of u and h (first MDI set). Thus, DGKS set

$$\Delta u \equiv u_0 \qquad \text{and} \qquad \Delta h \equiv h_0.$$

DGKS derived the following connection formula

$$\Delta\bar{\nu} = \nu \int_0^1 [\mathcal{K}_u \frac{u_0}{u} + \mathcal{K}_h \frac{h_0}{p}] d\tau, \tag{7}$$

where τ is the acoustic radius.

$$\tau = \int_0^r \frac{dr'}{c} [\int_0^R \frac{dr'}{c}]^{-1}.$$

The explicit forms of $\mathcal{K}_u$ and $\mathcal{K}_h$ are given in DGKS.

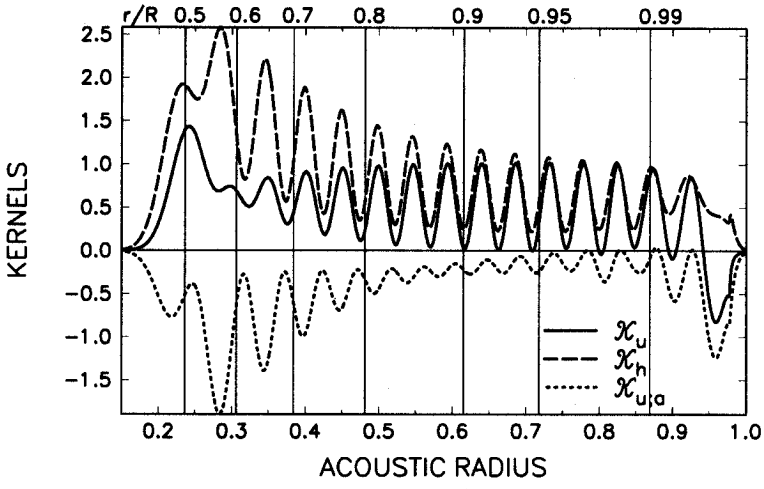

Fig. 3. Kernels, K_u, $\mathcal{K}_h$ and $\mathcal{K}_{u;a}$ vs. the acoustic radius and fractional radius, from DGKS. The kernels are for ℓ=20, $\nu \sim 3$ mHz and n=15.

For the splitting coefficients which reflect the non-spherically symmetrical part, DGKS made an approximation. The approximation is to ignore one term which can only be appreciable near the lower turning point. This term mixes the h_k term with its counterparts of lower rank. This term arises from the modification of the Lorentz force by the oscillations. In this way, DGKS obtained

$$a_{2k} \cong C_{k,s}\nu \int \mathcal{K}_{u;a}\frac{u_k}{u}d\tau. \tag{8}$$

The explicit form of $\mathcal{K}_{u;a}$ is given in DGKS. DGKS find that the inversions of equation (8) are not nearly so accurate as those of equation (7).

In Figure 3, we show examples of the three kernels in equations (7) and (8) for ℓ=20, ν=3 mHz and n=15. This is Figure 10 in DGKS. *The important thing to notice is that throughout most of the interior, the two kernels, $\mathcal{K}_u$ and $\mathcal{K}_h$, are very similar. This sends a rather grim message about the prospect of disentangling the magnetic field and temperature perturbations by simultaneous inversion. This is why we need guidance from observations in formulating the inversions. With proper guidance, we can make a better choice than what we are now forced to do.*

Because of the similarity between the two kernels, $\mathcal{K}_u$ and $\mathcal{K}_h$, DGKS did not attempt to solve a simultaneous inversion problem. Rather, they solved separate inverse problems, ignoring respectively the u_0, and then the h_0, contribution. Obviously, attributing all of the effect to only one type of perturbation can only place upper limits on the respective magnetic and "thermal" effects.

To determine how precise an outer condition is provided by the magnetic field, DGKS used BBSO Ca II K data their magnetic proxy. In Figure 4, we show their Figure 7. The figure depicts a series of Legendre decompositions of successive quarterly averages of daily BBSO Ca II K images using one image per day. Each image is projected onto the N-S axis, and the sum is then projected onto even Legendre coefficients. The overall normalization is arbitrary. The figure also shows the corresponding γ's from the MDI data for P_2, P_4, and P_6 coefficients of that decomposition. We do not show the k=0 term because of problems in absolute calibration of β_0. In Figure 4, there is a systematic correlation between the $\beta's$ of the quarterly Ca K data and the corresponding $\gamma's$. The strongest correlation is between the P_6 terms. The rough agreement continues through P_{10} (not shown). But there are differences for even the lowest degree coefficients. For example, at activity minimum (1996), the Ca II K signal is zero for all coefficients. However, the P_4 distortion in the MDI data is quite strong and persistent. Does this argue for another origin for the P_4 distortion? Like a thermal shadow?

We will see in the next section that the differences in Figure 4, are most likely due to inadequacies of the typical, synoptic measures of surface proxies for the field. Here we argue that the best determination of the outer boundary condition for the inversions comes from the BBSO Solar Disk Photometer (SDP).

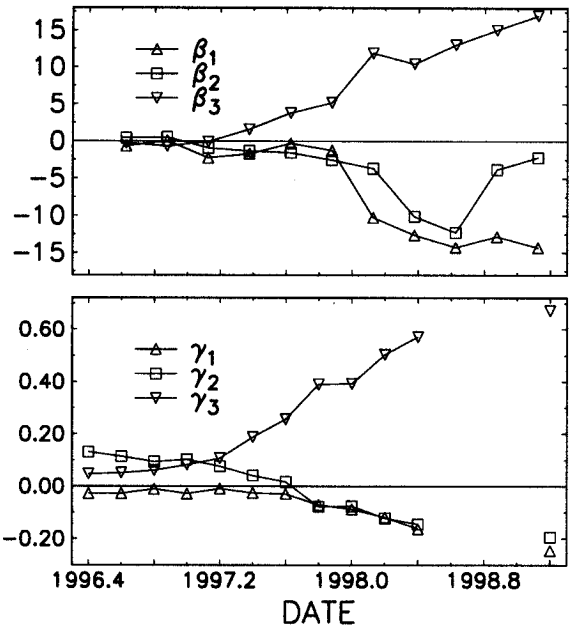

Fig. 4. Upper panel shows the quarterly P_2, P_4 and P_6 distortions in the BBSO Ca II K data. The $\beta's$ are from a Legendre fit of the daily images projected on the axis of rotation, and the ordinate is in arbitrary units. The error bars are within the symbols. The lower panel shows the corresponding $\gamma's$ (μHz) from the MDI data, see DGKS.

GUIDING THE INVERSIONS WITH BBSO SOLAR DISK PHOTOMETER (SDP) DATA

The SDP Instrument and Data

The Solar Disk Photometer (SDP) project was begun in the early 1990s with the aim of understanding the origin of solar irradiance variations. The SDP instrument (Taylor et al., 1998) is a re-designed version of the Mt. Wilson Limb Photometer which was used to determine the solar oblateness. Both photometers form an image of the Sun on an occulting disk which blocks all but a thin, annular portion of the image. The passed light is further blocked by a rapidly-rotating scanning disk with a single, radial slot to select light coming from a definite position angle on the annulus. The light is then passed through broad-band optical filters and collected by photodiodes. Whereas the Limb Photometer scanned only the limb, the SDP image size can be varied, via a commercial zoom lens, thereby permitting the solar disk to be scanned over a range of heliocentric angles. This feature enables the center-to-limb variation in the brightness contrast of solar features to be determined.

The SDP retains the essential features of the Limb Photometer, which enable relative photometry to be performed at the parts in 10^4 level. In particular, the telescope rotates about its axis on a regular schedule through the observing day. By combining data from different telescope orientations, the effect of imperfections arising in the telescope is strongly suppressed. The annular image is scanned at the rate of $\approx$ 100 Hz, which provides the averaging needed to suppress the effects atmospheric seeing and other rapid variations. The use of a single photodiode (per color channel) greatly reduces systematic problems caused by detector gain variations.

During a typical observing day SDP intensity data are recorded at 1024 positions around the annulus and at typically six different zoom settings, corresponding to the range $0 < \mu < 0.55$ of heliocentric cosine. Three color channels, centered at 0.43, 0.54, and 0.65 μm are employed, We work with the data in form of contrast values

$$\frac{\delta I}{I}(\phi_i, \lambda_j, \mu_{j,k}, t),$$

where $\phi_i, i = 0, 1023$ denotes position around the annulus, $\lambda_j, j = 0, 2$ denotes color channel (red, green, blue,

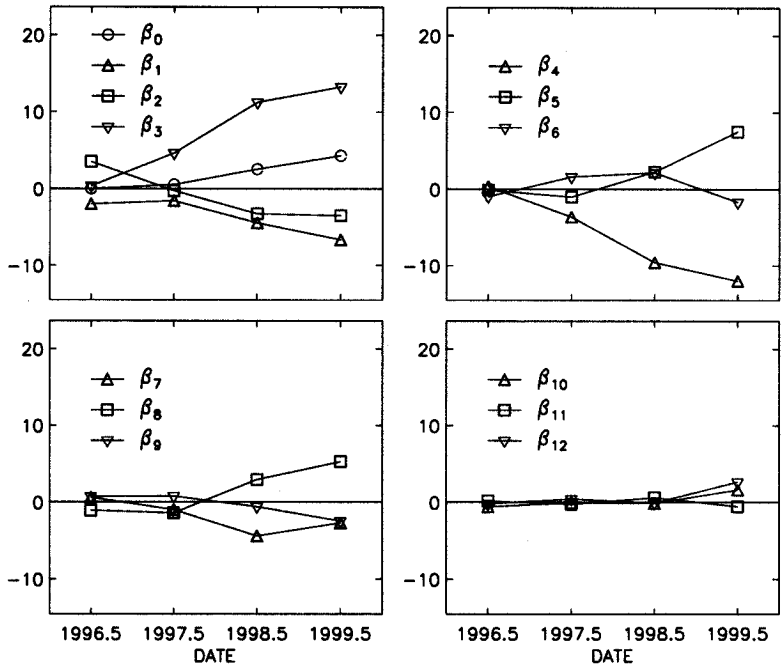

Fig. 5. Mean asphericity coefficients, β, (in degrees K) from the averages over the SDP data from 1996, 1997, 1998 and 1999 from the magnetic signal. The error bars are within the symbols. The plot shows $\beta_i \equiv b_{2i}$, from equation (9), for $i = 0, .., 12$ as a function of time. (Note that we arbitrarily referenced the coefficient of the P_0 term to epoch 1996.5 in making the plot.)

respectively), and $\mu_{j,k}, k = 1, 6$ is the heliocentric cosine of the annulus for color channel j and zoom setting k, at time t. Thus far, seven consecutive seasons (1993-9) of disk photometer data have been obtained.

The photometer is an ideal device from which one can extract both the sun's magnetic (facular) and thermal (intensity after removal of facular) signals.

Analyzing the SDP Data

To compare the photometric and helioseismic data we expand the latitude dependence of the former in Legendre polynomials. The first step in the analysis was to average the data samples of a given season for each zoom setting, color, and position angle. For a particular season, this average will be denoted

$$\frac{\delta I}{I}(\phi_i, \lambda_j, \mu_{j,k}).$$

The next step was to remove Fourier harmonics 0-2 from the ϕ dependence of the signal, for each λ and μ, as these harmonics contain large, non-solar components. We attempted to restore the solar component of the low harmonics as follows. The amplitude of the solar contribution to the 2nd harmonic is fixed by assuming that the solar $\delta I/I$ is the same at the equator and poles (as the signal is generally small there). The phase of the 2nd harmonic is set to zero, in accordance with the assumption that time-averaged solar activity is not a function of longitude. After restoring the 2nd harmonic signal, the 0th harmonic contribution is adjusted to raise the minimum value of $\delta I/I$ around the annulus to zero. In effect, we take the minimum value of $\delta I/I$, which occurs at high latitudes, to represent the quiet Sun. For reasons of symmetry, we make no correction to the 1st harmonic.

We then averaged the data from the east and west limbs and remapped the signal to a sine-latitude grid,

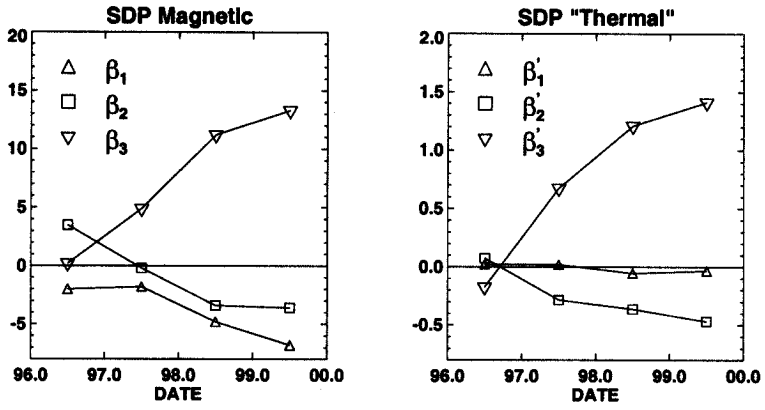

Fig. 6. Both panels show a Legendre decomposition of the SDP data for 1996-1999 including P_2, P_4 and P_6 distortions. The effect of spots is removed from both panels. The left panel includes the facular signal and the right panel has the facular signal removed. The error bars are within the symbols. The y-axis is in degrees K.

which yielded data in the form

$$\frac{\delta I}{I}(x_i, \lambda_j, \mu_{j,k})$$

for each season, where x is the sine of the solar latitude. is not a function of longitude. (We ignore the solar B angle in our analysis.)

The remainder of the present analysis was performed on the data from the blue channel for $\mu = \mu_{2,5} \approx 0.1$. Since the focus of this work is on the non-sunspot contribution to the irradiance we should have removed the sunspot contribution to $\delta I/I$. However, since we estimate the spot component to be less than $\sim 10\%$ of the blue signal near the limb, we made no correction.

We then converted the signal of interest to a latitude-dependent effective temperature perturbation, $\delta T(x)$, under the assumption that the observed emission has a thermal spectrum. Finally, to compare with the seismic results, we expanded the mean limb temperature perturbation for each season in Legendre polynomials, see Figure 5, as

$$\delta T(x) = \sum_{n=0}^{31} b_n P_n(x). \tag{9}$$

The Magnetic Boundary Condition from the SDP

In Figure 5, we show the Legendre decomposition of the BBSO SDP data which is dominated by the facular signal. The facular signal is the SDP proxy for the surface magnetic field. This decomposition measures the evolution of the solar asymmetry in degrees K. The typical observing season is about six months, centered on the summer. The figure shows a single point for each Legendre coefficient for each season. What is interesting is to compare this with the MDI signal shown in Figure 1.

The agreement between the β's from the SDP and the γ's from MDI is quite spectacular. In fact, there is good agreement from P_0 through P_{24}. Focussing on P_4, we see this component is strong in both measures – unlike the decomposition of the Ca II data. In fact, the higher degree Legendre coefficients in β show less structure than their counterparts in γ. It could be that the photometer data are superior here. Note that the errors the β's are smaller than those for the γ's. In fact, the error bars even for β_{12}'s (P_{24}'s) are within their symbols. Taken in total, one sees compelling evidence of the role of the field in the sub-surface perturbation driving the cycle dependent changes in the sun. However, this does not close the case. We need to show, by inversions, that the field is consistent with the observations of Lin (1995) and Lin and Rimmele (1999). Further, we need to determine the β's for the thermal signal from the SDP data.

Kuhn (1988, 1998) has argued that a thermal perturbation is causal in the changes. In the context of the SDP data, "thermal" means the residual signal after the removal of the facular contrast. Removing

the facular contrast is not a simple matter. Our very preliminary result for this is shown in Figure 6. The coefficients are given in degrees K. One can see that the thermal signal is about an order of magnitude smaller than the facular signal in Figure 5. We note that the results in Figure 6 are insensitive to whether or not we remove the sunspot signal. In the determination of coefficients in equation (9) for Figure 6, we used the method of Kuhn (1988) and Kuhn, Libbrecht and Dicke (1988), but we need to carefully check this result before presenting it as anything but a first cut which may be inaccurate.

Clearly, we are very close to having the required outer boundary condition needed to invert the MDI data for the nature of sub-surface perturbation causing the solar cycle changes so precisely manifest in the MDI data. Such guidance will motivate more sophisticated choices for the form of sub-surface perturbation.

ACKNOWLEDGEMENTS

This work was supported by NASA grants NAG5-9730 and NAG5-9682, and NSF grant ATM-97-14796.

REFERENCES

Bachmann, K. T. and T.M. Brown, P-mode Frequency Variation in Relation to Global Solar Activity, *ApJ,* **411**, L45, 1993.

Bhatnagar, A., K. Jain, and S.C. Tripathy, GONG p-Mode Frequency Changes with Solar Activity, *ApJ,* **521**, 885, 1999.

Dziembowski, W.A. and P.R. Goode, Seismology for the Fine Structure in the Sun's Oscillations Varying with Its Activity Cycle, *ApJ,* **376**, 782, 1991.

Dziembowski, W.A. and P.R. Goode, Effects of Differential Rotation on Stellar Oscillations - A Second-Order Theory, *ApJ,* **394**, 670, 1992.

Dziembowski, W.A., P.R. Goode, A.G. Kosovichev, and J.Schou, Signatures of the Rise of Cycle 23, *ApJ,* **537**, 1026, 2000.

Goldreich, P., N. Murray, G. Willette, and P. Kumar, Implications of Solar P-mode Frequency Shifts, *ApJ,* **370,** 752, 1991.

Howe, R., R. Komm, and F. Hill, Solar Cycle Changes in GONG P-Mode Frequencies, 1995-1998, *ApJ,* **524**, 1084, 1999.

Kuhn, J. R., 1988, Helioseismological Splitting Measurements and the Nonspherical Solar Temperature Structure, *ApJ,* **331**, L131, 1988.

Kuhn, J. R., On the Origin of the Helioseismic Solar Cycle Variations, in Structure and Dynamics of the Interior of the Sun and Sun-like Stars, eds. S. Korzennik and A. Wilson, ESA, 871, 1998.

Kuhn, J. R., K.G. Libbrecht, and R.H. Dicke, The surface Temperature of the Sun and Changes in the Solar Constant, *Science,* **242**, 908, 1988.

Libbrecht, K. G. and M.F. Woodard, Solar-cycle Effects on Solar Oscillation Frequencies, *Nature,* **345**, 779, 1990.

Lin, H., 1995, On the Distribution of the Solar Magnetic Fields, *ApJ,* **446**, 421, 1995.

Lin, H. and T.R. Rimmele, The Granular Magnetic Fields of the Quiet Sun, *ApJ,*, **514**, L448, 1999.

Ritzwoller, M. H. and E.M. Lavely, A Unified Approach to the Helioseismic Forward and Inverse Problems of Differential Rotation, *ApJ,* **369**, 557, 1991.

Rosenthal, C.R. and D.O. Gough, Scattering and Multiple Scattering of Acoustic Waves in a Stratified Medium, in Proc. Symp. on Seis. of the Sun and Sun-like Stars, ed. E. Rolfe (ESA SP-286), 457, 1989.

Rosenthal, C.R., The Role of Photospheric Magnetic Fields in the Variation of Solar Oscillation Eigenfrequencies, *ApJ,* **438**, 434, 1995.

Schou, J., ApJ, **523**, L181, 1991.

Schou, J., J. Christensen-Dalsgaard, and M.J. Thompson, On Comparing Helioseismic Two-dimensional Inversion Methods, *ApJ,* **433**, 389, 1994.

Spruit, H. , Solar Irradiance Variations: Theory, in International Astronomical Union. Symposium no. 185. New Eyes to See Inside the Sun and Stars, eds. Franz-Ludwig Deubner, Joergen Christensen-Dalsgaard, and Don Kurtz. Kyoto, Japan, 18-22 August, 1997, 103, 1998.

Taylor, S.F., J.R. Varsik, M.F. Woodard, and K.G. Libbrecht, Spatial Dependence of Solar-Cycle Changes in the Sun's Luminosity, *Solar Phys.,* **178**, 1, 1998.

Tomczyk, S., 1996, private communication

Woodard, M. F. and K.G. Libbrecht, Is There an Acoustic Resonance in the Solar Chromosphere?, *ApJ*, **374**, L61, 1991.

Zweibel, E.G. and W. Däppen, Effects of Magnetic fibrils on Solar Oscillation Frequencies - Mean Field Theory, *ApJ*, **343**, 991, 1989.